Stability of vacancy-hydrogen clusters in nickel from first-principles calculations

Döme Tanguy, Yu Wang, Damien Connétable

Stability of vacancy-hydrogen clusters in nickel from first-principles calculations

Döme Tanguy [a,*], Yu Wang [a,b], Damien Connétable [b]

[a] *Institut Lumière Matière, UMR5306 Université Lyon 1—CNRS, Université de Lyon, 69622 Villeurbanne Cedex, France*
[b] *CIRIMAT, CNRS-INP-UPS UMR 5085, École Nationale d'Ingénieurs en Arts Chimiques et Technologiques (ENSIACET) 4, allée Émile Monso, BP 44362, F-31030 Toulouse Cedex 4, France*

Abstract

The interactions of hydrogen (H) atoms with vacancies are investigated by means of ab initio calculations. The lowest segregation energies are −0.27 and −0.41 eV at single vacancies and divacancies, respectively. These values are in excellent agreement with those corresponding to the two characteristic peaks of the thermal desorption spectra. The microscopic interpretation of the experimental data is therefore clarified. An energetic model is built from the ab initio data and used to study the influence of H bulk concentration and temperature on the concentration of vacancy-H clusters. Analytical expressions, validated by Monte Carlo simulations, are given. The mean vacancy occupation and the H-induced vacancy enrichment are calculated at two temperatures representative of H embrittlement experiments and stress corrosion cracking at high temperatures. The stability domain of VH_6 clusters is found to significantly overlap with the experimental conditions for embrittlement. Therefore, vacancy clustering at high concentrations can be qualitatively discussed based on VH_6–VH_6 interactions that are found weakly repulsive. Consequences on H damage in Ni are discussed. The effect of metal vibrations on segregation and local hydride stability is qualitatively evaluated by off-lattice Monte Carlo simulations using a semi-empirical Ni–H potential. They are shown to shift local hydride stability towards higher H concentrations.

1. Introduction

The interactions of hydrogen (H) with point defects in metals have been intensively studied [1]. The motivation is to understand the complex interplay between H and the microstructure. This research could lead to physically based models of damage in H-generating environments and help design new materials resistant to extreme conditions, such as plasma-facing materials [2]. Ion implantation [3] has been used to study deuterium (D)–vacancy interactions in Ni. This process creates all sorts of point defect–H clusters at low temperature, the most stable being vacancy–H clusters. Ion channeling showed that the preferred H position in the vacancy is the octahedral site, which enables multiple occupancy. Binding energies have been extracted from thermal desorption data by simulating D release with parametrized diffusion equations including trapping. Two characteristic energies were found the significance of which on the microscale needs to be established. In many systems, the binding energies have been calculated ab initio [4–7], but in Ni interpretation of the experiments still relies on the semiquantitative effective medium theory [8] and a consensus has not been reached yet [9]. We present here ab initio results that clarify this situation.

Furthermore, Fukai showed that at high H concentration, most metals should be considerably enriched with vacancies (called superabundant vacancies (SAVs) [1])

* Corresponding author.
  E-mail address: dome.tanguy@univ-lyon1.fr (D. Tanguy).

when they approach thermodynamic equilibrium. The reason is that strong binding and multiple occupancy can compensate the formation energy of the defect. In Ni [9,10], at high H pressure and high temperature, the enrichment is gigantic. X-ray diffraction peaks indicate the ordering of the vacancies in the $L1_2$ structure at 25% vacancy concentration. An important issue is whether these SAVs play a role in the environmental degradation of Ni-based alloys. For example, at room temperature, a possible role of out-of-equilibrium vacancies, produced by plastic deformation and stabilized by H, on the grain boundary (GB) cohesion has been proposed [11,12]. Another aspect is enhanced substitutional solute transport due to the increase in vacancy concentration. This, in relation to oxidation, is important for the nuclear industry. More precisely, the susceptibility of alloy 600 to stress corrosion cracking in pressurized water reactors (PWRs) is a major concern in terms of extending the life of these nuclear plants. The intergranular crack propagation mechanism is not fully understood although much has been learned from transmission electron microscopy observations [13,14]. Cracks grow concomitantly with the formation of a Cr_2O_3 oxide. Oxygen diffusion through the oxide from the external medium and Cr diffusion from the material towards the oxide tip seem to be the key mechanisms. However, the role of local strain is not explained and other mechanisms could play direct or indirect roles. For example, absorbed H, produced during depassivation/repassivation events [15,16], could directly embrittle the GBs or participate indirectly by enhancing Cr transport via SAV formation. It was shown by Ni/Cu interdiffusion experiments [17] that SAVs can indeed increase diffusion by many orders of magnitude. This phenomenon is not limited to H: impressive nanoscale interdiffusion profiles were recently produced by atom probe tomography that show carbon-enhanced Ni diffusion in Fe [18]. The measurements are not in agreement, so far, with the modeling of α-Fe self-diffusivity in the presence of C–vacancy clusters [19,20] predicting a slow down. The discussion of this discrepancy [21] highlights the necessity to develop robust models that predict the concentrations of vacancy–interstitial solute clusters since these appear as a multiplicative factor in the self-diffusion coefficient.

In this context, it seems useful to derive, from first principles, the average H occupancy of out-of-equilibrium vacancies and SAV content over a range of H concentrations and temperatures relevant to applications in Ni. The paper is organized as follows: The methods (ab initio calculations and Monte Carlo simulations) are presented. The energies characteristic of H interaction with vacancies are given and the coherency with experiments is established. Then, the influence of temperature and bulk H concentration on the VH_n cluster distribution is obtained by minimization of a free energy functional based on energies mentioned above (ab initio). The robustness of the functional is based on a quantitative comparison with Monte Carlo simulations (MC) "on a lattice", based on the same energetic model. The influence of the metal vibrations on segregation energies and H–H pair interactions is evaluated by off-lattice Monte Carlo (OLMC) simulations. This refinement requires a lengthy comparison between the semi-empirical interatomic potential used in OLMC and the ab initio data. It should not distract the reader from the essential message that is carried by the lattice model. Finally, the implication of VH_n for environmental damage is discussed.

2. Methods

The calculation of the energy of the basic vacancy–H configurations are performed using the Vienna Ab initio Simulation Package (VASP) [22] The Kohn–Sham equations are solved by means of the projected-augmented wave (PAW) method [23] to describe the electron–ion interactions, and the Perdew–Wang (PW 91) approximation [24] for the exchange and correlation functionals. Magnetic moments are taken into account in all calculations. $3 \times 3 \times 3$ supercells are used to study the VH_n clusters, and to determine the VH_6–VH_6 interactions, $4 \times 4 \times 3$ supercells are used to reduce image interactions (divacancies are in the x-y plane). The cut-off energy is maintained at 450 eV, and $6 \times 6 \times 6$ and $5 \times 5 \times 6$ Monkhorst–Pack grids [25] are used to sample the Brillouin zone, according to the size of the supercell.

Zero point energy (ZPE) corrections are evaluated by diagonalizing the dynamic matrix corresponding to the degrees of freedom of H only.

In a second step, the influence of temperature and bulk hydrogen concentration on the mean occupancy of the vacancy interstitial sites is evaluated. Different degrees of details are retained to calculate the potential energy of the system. First, we consider a lattice model where H can occupy only the octahedral (O) sites of the face-centered cubic (fcc) Ni and the tetrahedral sites (T_1) inside a single vacancy (Fig. 1) placed in a crystal containing N metal sites ($N = 256$, 2048, 16384, 131072 and 1048576). The energy of the configurations is evaluated from the minimum number of segregation energies and pair interactions between the interstitial sites of the vacancy (O_1, O_2, T_1, Fig. 1), extracted from the energy of relevant configurations, calculated by DFT. The average occupancies and equilibrium VH_n fractions are calculated analytically using mean field equations, validated by equilibrium MC simulations in the canonical ensemble. These simulations are done "on a lattice" (i.e. by proposing only lattice site changes to the H atoms) using the same energetic model. The absolute vacancy concentration is obtained by the same equations in the grand canonical ensemble. Second, the influence of the vibrational entropy, and of long-range vacancy–H interactions, is investigated using a semi-empirical, continuous, interatomic potential. The EAM Ni–H potential from Angelo and Baskes [26], after validation, is used to perform off-lattice MC simulations [27]. The volume is relaxed by performing dilatation moves, and the metal particles are
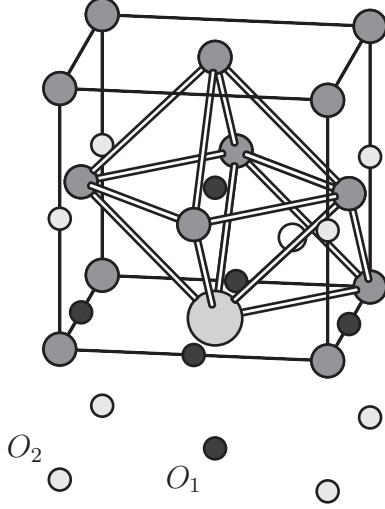
Fig. 1. A vacancy in a face-centered cubic structure surrounded by the first and second shell of octahedral sites (6 O_1 and 8 O_2 sites) and only one, out of eight, T_1 tetrahedral interstitial sites represented (white ball).

thermally excited by random displacement increments, selected uniformly with a prescribed maximum amplitude. H is considered as a classical particle in this model and is also thermally excited. Similar to MC "on the lattice", exchange moves are also performed to sample the H configurations.

3. Interactions between a vacancy and a hydrogen atom in Ni

In this section, the site-dependent segregation energies (ΔE_{seg}^i, where i is the label of the site) and H–H pair interactions (ϵ_{ij}, where j is the label of a neighbor of site i) are calculated. The binding energy is defined, per H atom, by:

$$E_n^b = (E_o[(N-1).Ni + n.H] - E_o[(N-1).Ni])/n$$
$$- (E_o[N.Ni + H_{octa}] - E_o[N.Ni]) \quad (1)$$

where n is the number of H atoms in the vacancy and the reference state ($E_o[N.Ni + H_{octa}]$) is the energy of the supercell with one H atom on a bulk octahedral site (O_b) and N Ni atoms. When n equals 1, E_1^b is the segregation energy. The values are given for sites O_1, T_1 and O_2 in Table 1. O_1 is the strongest trap, in particular when ZPE is considered, but T_1 is also favorable. The values are small (and oscillating) beyond the second shell of neighbors [28]. For n larger than 1, E_n^b is configuration dependent because of H–H interactions.

Only the average binding energies, as a function of n, are reported (see Table 2). The average is weighted by the number of equivalent configurations. A detailed presentation of all possible H distributions over the sites of the vacancy, the corresponding energy and number of equivalent combinations can be found elsewhere [28] and shows a similarly weak configurational dependency. The focus is here on clusters composed of occupied O_1 sites only. The values (Table 2) are almost constant; therefore, as an approximation, the interaction between O_1 sites is neglected in the lattice model, i.e. $\varepsilon_{O_1 O_1}$ is set to zero. Note that the segregation energy itself (in comparison to the binding energy, which is the average of the segregation energy over all H contained in the vacancy) shows a more pronounced configuration dependence. Nevertheless, we are interested in the distribution of the clusters, which is obtained from their formation energy, and making the simplification of taking a constant segregation energy, we make only a small error on the formation energy (in between 0.003 and 0.045 eV).

Next, $\varepsilon_{T_1 T_1}$ can be extracted from the energy of a VH_2 cluster with T_1–T_1 first neighbor interactions. The segregation energy is −0.245 eV for the first H and −0.026 eV for the second. By definition, $\varepsilon_{T_1 T_1}$ is the difference between these energies, which gives +0.22 eV. In a similar way, $\varepsilon_{O_1 T_1}$ can be extracted from the value of the segregation energy when a second H atom is brought from the bulk to an T_1 site in the first neighbor position of an occupied O_1 site (-0.012 eV). Knowing that $\Delta E_{seg}^{O_1}$ is −0.259 eV gives $\varepsilon_{O_1 T_1}$ equal to +0.247 eV. There is a configuration dependence, but without consequences. It is therefore ignored.

So far, only interstitial sites inside the vacancy have been considered. It will be shown below that due to the slightly lower segregation energy on O_1 compared to T_1 and the strong repulsion between them, only O_1 sites are occupied away from the dilute limit. Therefore, when all O_1 sites are saturated (VH_6 configuration), the only way to enrich the cluster further is by filling O_2 sites. The corresponding segregation energies are given in Table 3. The pair interaction $\varepsilon_{O_1 O_2}$ is defined in this case by:

$$\Delta E_{seg} = \Delta E_{seg}^{O_2} + 3\,\varepsilon_{O_1 O_2} \quad (2)$$

and is also shown in Table 3 as a function of the number of occupied O_2 sites. O_2 sites are considered sufficiently far apart to have negligible interactions. Therefore, the values are not configuration dependent. $\varepsilon_{O_1 O_2}$ in Table 3 is almost constant and is approximated by −0.05/3 eV.

Finally, a simple atomic picture emerges: segregation on T_1 and O_1 is strong, with a slight preference for O_1 ($\Delta E_{seg}^{O_1} = -0.273 eV$), and moderate on O_2 ($\Delta E_{seg}^{O_2} = -0.05eV$). There is almost no interaction in between O_1 sites

Table 1
Binding energy (E_1^b, in eV), the zero point energy correction (ΔE^{ZPE} in eV) and the segregation energy ($\Delta E_{seg} = E_1^b + \Delta E^{ZPE}$), for the various sites in the vicinity of the vacancy.

Site	E_1^b	ΔE^{ZPE}	ΔE_{seg}
T_1	−0.245	0.023	−0.222
O_1	−0.259	−0.014	−0.273
O_2	−0.050		

Table 2
Average binding energies ($\overline{E_n^b}$ in eV) for clusters containing only occupied O_1 sites, without ZPE.

VH_1	VH_2	VH_3	VH_4	VH_5	VH_6
−0.259	−0.258	−0.250	−0.255	−0.250	−0.263

VH_n	ΔE_{seg}	$3 \times \varepsilon_{O_1 O_2}$
VH_7	−0.1	−0.05
VH_8	−0.102	−0.052
VH_9	−0.115	−0.065
VH_{10}	−0.105	−0.055
VH_{11}	−0.117	−0.067
VH_{12}	−0.109	−0.059
VH_{13}	−0.097	−0.047
VH_{14}	−0.092	−0.042

and a strong, short-range, repulsion between O_1 and T_1 and in between T_1 sites in first neighbor position. These results contrast with those from effective medium theory [8], which overestimates segregation on O_1 (-0.4 eV) and predicts a strong repulsion between H atoms on O_1 sites (segregation energy should go up to −0.2 eV when O_1 sites in first neighbor position are occupied). Furthermore, we found [28] that two vacancies in the first neighbor position offer two octahedral positions with an enhanced segregation of −0.405 eV (−0.41 including the ZPE). Our results coincide remarkably with the values obtained from thermal desorption of deuterium implanted [3] or thermally treated under high H pressure [29] samples: −0.27 and −0.43 eV, which confirms the interpretation of two independent traps—one being the single vacancy and the stronger one being the divacancy [3,9]. In the next sections, we go further by predicting, from the DFT segregation energies and H–H pair interactions, the stability of the H–vacancy clusters as a function of T and C_H. After showing the stability domain of VH_6, we calculate the effective cluster interactions for VH_6–VH_6 in the first and second neighbor positions to indicate how they order at high concentration, in the light of the experimental results obtained at high temperature.

4. Stability of VH_n

We now calculate the equilibrium distribution of the VH_n clusters as a function of thermodynamic conditions from the parameters ($\Delta E_{seg}^{O_1}$, $\Delta E_{seg}^{O_2}$, $\Delta E_{seg}^{T_1}$, $\varepsilon_{T_1 T_1}$, $\varepsilon_{O_1 O_1}$, $\varepsilon_{O_1 O_2}$) obtained ab initio in the previous section. Two situations are considered: an "out-of-equilibrium" vacancy embedded in a homogeneous hydrogen field, or full equilibrium where the system can modify its vacancy content, in the presence of H.

In this first case, we can write a free energy functional parameterized only by the mean occupancies of the interstitial sites in the system. The mean potential energy, in the Bragg–Williams approximation, as a function of the mean site occupancies C_{O_1}, C_{T_1}, C_{O_2} and C_{O_b} is:

$$U(C_{O_1}, C_{T_1}, C_{O_2}, C_{O_b}) = U_0 + 6[C_{O_1}\Delta E_{seg}^{O_1}$$
$$+ 4C_{O_1}C_{T_1}\varepsilon_{O_1 T_1}/2$$
$$+ 4C_{O_1}C_{O_2}\varepsilon_{O_1 O_2}/2]$$

$$+ 8[C_{T_1}\Delta E_{seg}^{T_1} + 3C_{T_1}C_{O_1}\varepsilon_{O_1 T_1}/2 + 3C_{T_1}C_{T_1}\varepsilon_{T_1 T_1}]$$
$$+ 8[C_{O_2}\Delta E_{seg}^{O_2} + 3C_{O_1}C_{O_2}\varepsilon_{O_1 O_2}/2] \qquad (3)$$

The integers 6, 8 and 8 in Eq. (3) are the numbers of geometrically equivalent sites (O_1, T_1 and O_2 respectively) and U_0 is a configuration-independent energy. Then, by adding the ideal configurational entropy and lifting the constraint of a fixed total number of H atoms (n_H) by introducing the chemical potential (μ_H), the free energy functional is:

$$F_{(N-1,n_H,V,T)}(C_{O_1}, C_{T_1}, C_{O_2}, C_{O_b}) - \mu_H n_H = U(C_{O_1}, C_{T_1}, C_{O_2}, C_{O_b})$$
$$+ k_B T [6(C_{O_1}\ln(C_{O_1}) + (1-C_{O_1})\ln(1-C_{O_1}))$$
$$+ 8(c_{T_1}\ln(C_{T_1}) + (1-C_{T_1})\ln(1-C_{T_1}))$$
$$+ 8(c_{O_2}\ln(c_{O_2}) + (1-C_{O_2})\ln(1-C_{O_2}))$$
$$+ (N-6-8)(C_{O_b}\ln(C_{O_b})$$
$$+ (1-c_{O_b})\ln(1-C_{O_b}))]$$
$$- \mu_H(6C_{O_1} + 8C_{T_1} + 8C_{O_2} + (N-6-8)C_{O_b}) \qquad (4)$$

where N is the number of fcc sites in the system. Minimizing the functional gives the segregation equations:

$$\frac{C_{O_b}}{1-C_{O_b}} = e^{\mu_H/k_B T} \qquad (5)$$

$$\frac{C_{O_1}}{1-C_{O_1}} = e^{-(\Delta E_{seg}^{O_1} + 4C_{T_1}\varepsilon_{O_1 T_1} - \mu_H)/k_B T} \qquad (6)$$

$$\frac{C_{T_1}}{1-C_{T_1}} = e^{-(\Delta E_{seg}^{T_1} + 3C_{O_1}\varepsilon_{O_1 T_1} + 3C_{T_1}\varepsilon_{T_1 T_1} - \mu_H)/k_B T} \qquad (7)$$

$$\frac{C_{O_2}}{1-C_{O_2}} = e^{-(\Delta E_{seg}^{O_2} + 3C_{O_1}\varepsilon_{O_1 O_2} - \mu_H)/k_B T} \qquad (8)$$

Figs. 2 and 3 show the numerical solution of these equations at $T = 300$ and 600 K, respectively. It can be observed that even if O_1 and T_1 have similar segregation energies (with a small preference for O_1), only the O_1 site is occupied, due to the strong O_1–T_1 repulsion. Monte Carlo simulations, on the lattice, show that this effect is overestimated by the mean field treatment (especially at low temperature). Indeed, if no

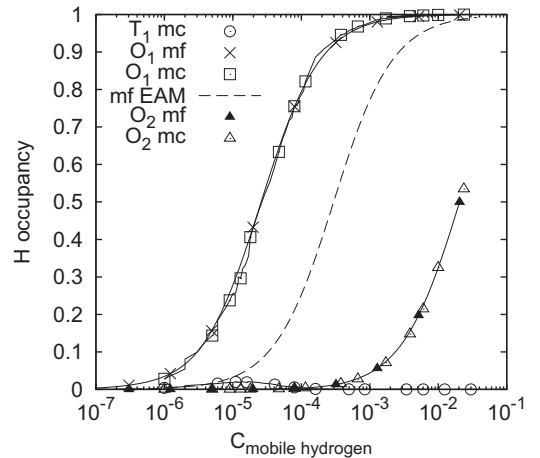Fig. 2. Variation of the vacancy site occupancies as a function of the bulk H content C_{O_b} ($C_{\text{mobile hydrogen}}$) at $T = 300$ K, obtained by the mean field equations (mf) and by Monte Carlo simulations (mc) using the energetic model based on DFT.
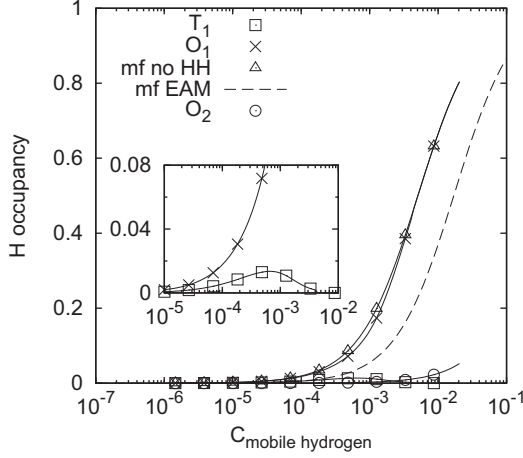
Fig. 3. Variation of the vacancy site occupancies as a function of the bulk H content C_{O_b} at $T = 600$ K, obtained by the mean field equations (mf). Monte Carlo simulations give very similar results.

more than one O_1 is occupied, it is possible to put a second H on a T_1 site without interactions between the H atoms if they are far apart. The mean field approach, by averaging the concentration over all geometrically equivalent O_1 sites, ignores this possibility. Nevertheless, the occupancy of T_1 is always smaller than 0.02 and only occurs at low C_{bulk} (below 100 ppm at 300 K). This is coherent with ion channeling experiments which report only O_1 occupation [3]. The detail of the concentration of the different cluster species is given in Fig. 5, from Monte Carlo simulations and analytical Eq. (10). The agreement is excellent and not straightforward since O_2 sites had to be considered to achieve a quantitative agreement at high temperature and high H concentration. At low temperature, VH_6 can be formed at low H concentrations (below 100 ppm) and at 1000 ppm more than 80% of vacancies are saturated with H. This shows that vacancy diffusion crucially depends on H in these conditions typical of H embrittlement of Ni [30,12]. On the contrary, at $T = 600$ K, free vacancies still represent a significant fraction of the clusters (Fig. 6), which means that vacancy diffusion should not be affected so much, at least below 1000 ppm H concentration in the bulk.

At high concentrations and low temperature (Fig. 2), the occupancy of sites O_2 increases significantly, which is a sign of a precursor of a "local hydride". This occurs when O_1 is almost saturated; therefore segregation on O_2 is enhanced by $\varepsilon_{O_1O_2}$ and $\Delta E_{seg}^{O_2}$ equals -0.1 eV instead of -0.05 eV in the dilute limit. Nevertheless, saturation is far from being reached, even at 1% H (Fig. 2).

To go beyond the rigid lattice and short-range interactions approximations, we use OLMC simulations, with a continuous EAM potential. Fig. 4 presents the results of such simulations for three temperatures. A fit of the results by the mean field formulas, in the dilute limit, gives access to the segregation free energies. They are -0.185, -0.183 and -0.182 eV for 300, 450 and 600 K, respectively, to be compared to -0.21 eV at $T = 0$ K. The effect of the vibrational entropy is to shift the O_1 occupancy curve by half a

decade towards higher concentrations. In the EAM, the T_1 sites have a much higher energy than the O_1, but we have shown above that this has only a small impact on segregation. Contrary to DFT, the O_1 sites have repulsive interactions as can be seen from the segregation isotherm at $T = 300$ K that falls below the mean field curve when more than one H is in the vacancy ($C_{O_1} > 0.17$ on Fig. 4). At higher concentrations, the curve becomes steeper than the mean field, because of O_1 O_2 attractive interactions. The segregation energy on the O_2 site is -0.075 eV in the dilute limit and -0.12 eV when the O_1 sites are saturated. The effective pair interaction is therefore $-0.045/3$ eV, which is in very good agreement with DFT. Therefore, we can conclude that EAM reasonably describes the "nanohydride" stability, at least in the vicinity of the vacancy, with a slight tendency to overstabilize it: the segregation energy to an O_2 site close to VH_6 is -0.1 eV from DFT and -0.12 eV according to the EAM. Segregation on the O_1 site is underestimated with respect to DFT which shifts the occupancy by one order of magnitude towards the high concentrations, as shown in Fig. 2 (discontinuous curve). At $T = 300$ K, the concentration on O_2 and O_3 are significantly enhanced beyond 1000 ppm (insert of Fig. 4), but the increase is largely retarded in comparison to mean field equations (solid lines on the insert correspond to -0.12 and -0.075 eV). A fit to Eq. (8) gives a segregation free energy of -0.025 eV on site O_2 and a free pair energy O_1O_2 of $-0.05/3$ eV, vs. -0.075 eV and $-0.045/3$ at zero K. This reduction in the segregation energy due to vibrational entropy is responsible for a shift of the occupancy of sites O_2 towards higher bulk H concentration by a factor 7 at 300 K—an effect well known in substitutional alloys [31,32]—and therefore a delay in the formation of the local hydride. Vibrational effects were ignored in previous works
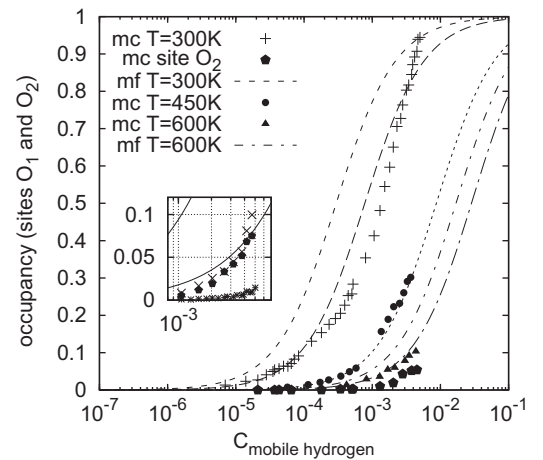

Fig. 4. Variation of the vacancy site O_1 occupancy with c_{O_b} obtained by off-lattice Monte Carlo simulations. The lines represent the mean field equations fitted on the MC results for three temperatures 300, 450 and 600 K. Two curves, labeled "mf", correspond to mean field equations for 300 and 600 K, using segregation energies obtained at 0 K. The insert shows the increase of the concentration on sites O_2, O_3 and O_4. Solid lines are the mean field equations for ΔE_{seg} equals -0.075 and -0.12 eV.

on local hydrides [33,34]. Nevertheless, the results should not be qualitatively changed especially at the crack tip where a fully formed hydride might not be necessary to switch off plasticity.

We now consider that the system can adjust the number of vacancies easily. Following Ref. [6], we rewrite the free energy functional as a function of all possible VH_n clusters. In the (μ_H, μ_M, V, T) ensemble, the grand potential is now, in the dilute limit:

$$\Omega = ME_M + \langle N_V \rangle (E_f - \mu_M)$$
$$+ \langle N_{VH_1} \rangle \left(E_f - \mu_M + \Delta E_{seg}^{O_1} \right) + \cdots$$
$$+ \langle N_{VH_k} \rangle \left(E_f - \mu_M + \sum_{i=1}^{k} \left(\Delta E_{seg}^i + \sum_j \varepsilon_{ij}/2 \right) \right)$$
$$- N\mu_M + n_H^{tot} E_H - n_H^{tot} \mu_H - TS \qquad (9)$$

where E_f is the vacancy formation energy; E_M is the potential energy per atom of the perfect crystal; μ_M is the chemical potential of the metal, which is approximately equal to E_M; ΔE_{seg}^i is the H segregation energy on site i, in the dilute limit; ε_{ij} is the effective H pair interaction between sites i and j. M is the number of metal sites in the crystal. $\langle N_{VH_k} \rangle$ is the average number of VH_k clusters in the crystal. Note that this is a generic cluster and that every distribution of H among the interstitial sites of the vacancy leads to a different term in the equation at that point. S is the ideal configurational entropy. E_H is the energy required to embed an H atom in the crystal, in the dilute limit. n_H^{tot} is the total number of H in the system, which is the sum of all the H in the various clusters and on the bulk sites. Minimizing the free energy with respect to all cluster concentrations gives the following expressions:

$$\frac{C_{bulk}}{1 - C_{bulk}} = e^{-\mu^*/k_BT}$$
$$C_V = e^{-E_f/k_BT} \qquad (10)$$
$$C_{VH_k} = n_{VH_k} e^{-\left(E_f + \sum_{i=1}^{k} (\Delta E_{seg}^i + \sum_j \varepsilon_{ij}/2) + k\mu^* \right)/k_BT}$$

where $\mu^* = E_H - \mu_H$; C_{bulk} is the H concentration on bulk octahedral sites that correspond to μ^*; C_{VH_k} is the concentration of clusters of type VH_k and n_{VH_k} is the number of different clusters that can be built by permutation of the H on the lattice sites, still having the same formation energy. All energy parameters are the same as above. The vacancy formation energy E_f is taken as 1.79 eV, from the experimental value obtained by positron annihilation [35]. In Ni, there is a large discrepancy in this quantity depending on the technique used, with values as low as 1.4 eV [36]. As a consequence, we will also consider that the formation energy can be much lower than 1.79 eV at the temperatures we consider. For each k value of Eq. (10), only the clusters that have the lowest formation energy are considered, i.e. those that have no repulsive H pair interactions. The details of all the configurations

considered are given in the Appendix. Essentially, the distribution of clusters obtained by MC simulations is quantitatively reproduced by the model, at low temperature, by considering only the O_1 and T_1 sites (Fig. 5). At high temperatures (Fig. 6) and high H content, in our case at $T = 600$ K and beyond 1000 ppm, one also has to include the configurations involving site O_2. Otherwise, the model underestimates VH_4, VH_5 and VH_6 by up to a factor 2. The variation of the equilibrium cluster concentration and the total vacancy enrichment are shown in Figs. 7 and 8. To highlight the surge in concentration due to the presence of H, the thermal vacancy concentration in the absence of H is added to every cluster concentration. As a result, an absence of clusters is represented by a horizontal line on the log–log plot and a deviation from the horizontal indicates an enrichment. At $T = 300$ K (Figs. 5 and 7), VH_1 begins to increase at about 0.1 ppm, while VH_6 are formed beyond 20 ppm. VH_n, $n < 6$, are the dominant species up to 100 ppm. Looking at the absolute equilibrium concentration of vacancies, the enrichment is large. For example, it is about 10 orders of magnitude with respect to the thermal vacancy concentration in the pure system at 300 K and 1000 ppm. Nevertheless, the total concentration of H–vacancy clusters is small, of the order of 10^{-20}. The total amount of H trapped is negligible. At 600 K (Fig. 8), the effect is even smaller. Taking the lower limit for the formation energy of the vacancy, 1.4 eV [36], which is also the result of the ab initio calculation with the approximations chosen here, shifts the concentrations upward by a factor 3×10^6 at 300 K and 2000 at 600 K, which does not change the message: the low equilibrium concentrations highlight the importance of out-of-equilibrium vacancies (studied above) in these thermodynamic conditions and the locations where the vacancy formation energy is low, e.g. GBs.

Another aspect is the effective interaction in between VH_6 clusters that dictates the phase-separation behavior. We focus on VH_6 interactions, because they are the most stable species at high concentration. When bringing together two of these clusters, a decorated divacancy may
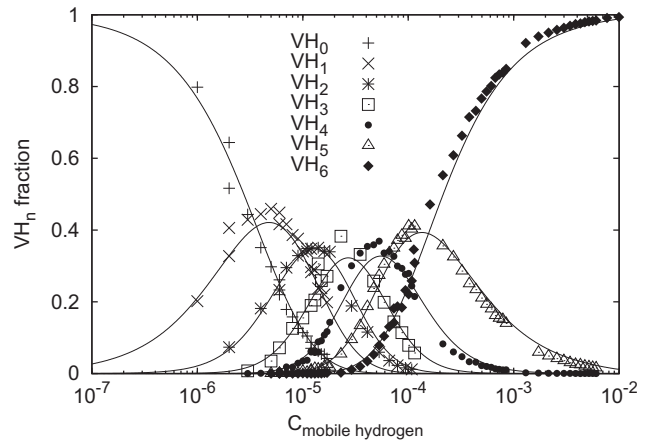

Fig. 5. Distribution of VH_n clusters at $T = 300$ K. Symbols correspond to Monte Carlo simulations and lines correspond to Eqs. (10).
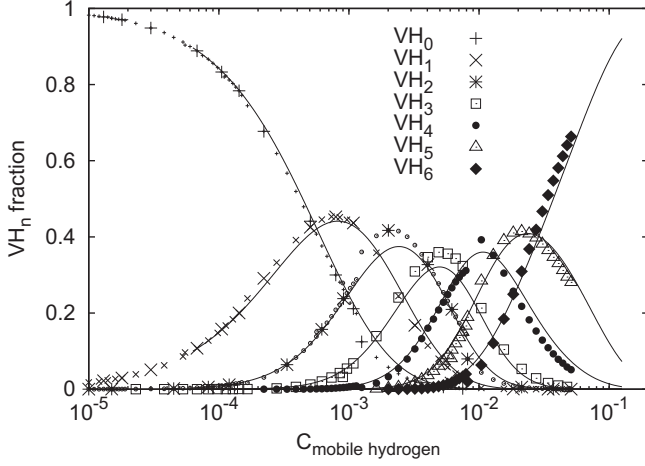
Fig. 6. Distribution of VH_n clusters at $T = 600$ K. Symbols correspond to Monte Carlo simulations and lines correspond to Eq. (10).
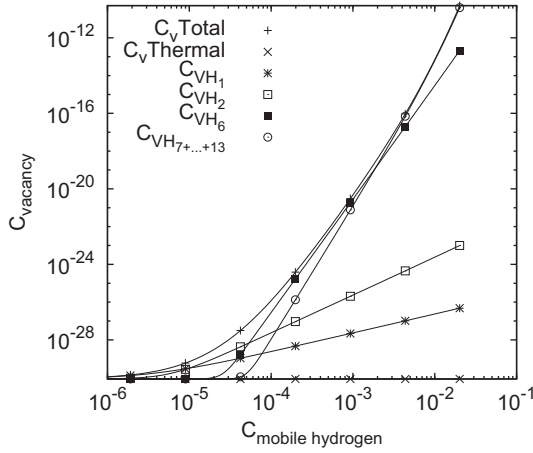

Fig. 7. Variation of the cluster concentration (added to the thermal vacancy concentration) at $T = 300$ K.
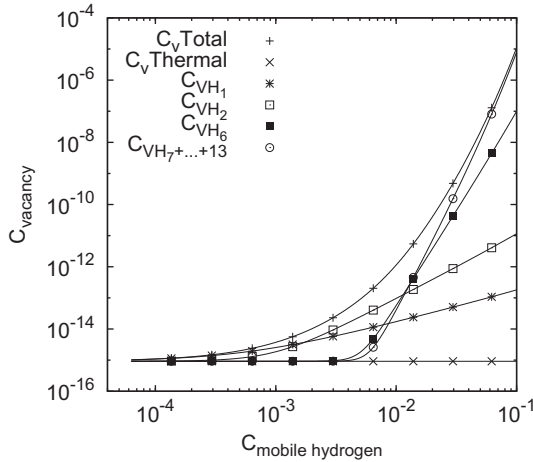

Fig. 8. Variation of the cluster concentration (added to the thermal vacancy concentration) at $T = 600$ K.

be formed. Without hydrogen, the two compact divacancies (the first nearest and next nearest neighboring vacancies, labeled 1NN and 2NN) have both negative binding

energies (approximately -0.1 eV), in favor of the 1NN divacancy (by approximately 10 meV). To form decorated divacancies, the two VH_6 clusters must eject one or two H atoms because octahedral sites overlap in the clusters. We consider 1NN and 2NN divacancies with all octahedral sites filled: in a 1NN cluster there are 10 (H atom) octahedral sites, i.e. V_2H_{10} is formed, and in 2NN there are up to 11 H atoms, V_2H_{11}. The effective interaction, taking as reference the VH_6, is given by:

$$\epsilon[V_2H_{10}] = E^f[V_2H_{10}] + 2E^f[H_{octa}] - 2E^f[VH_6] \qquad (11)$$

for V_2H_{11}, and:

$$\epsilon[V_2H_{11}] = E^f[V_2H_{11}] + E^f[H_{octa}] - 2E^f[VH_6] \qquad (12)$$

for V_2H_{11}. $E^f[V_2H_{11}]$ and $E^f[V_2H_{10}]$ correspond to the formation energy of the V_2H_{10} and V_2H_{11} clusters, respectively, and $E^f[H_{octa}]$ and $E^f[VH_6]$ to the formation energy of an H atom on a bulk octahedral site and of the VH_6 cluster. One finds $+10$ and $+40$ meV, respectively. The balance is slightly positive, which means that VH_6 do not cluster at low concentration, but remain in solid solution. The tendency is to not form L1$_2$ ordered domains at high concentration at low temperature and low pressure, in contrast with high-temperature experiments [29].

Finally, at $T = 1200$ K (not shown), concentrations of vacancies beyond 1% can be obtained but only for very high H concentrations (beyond 1%), which seems coherent with the observations of Fukai [1]. A quantitative comparison with Fukai's results would require the determination of the effect of high temperature and pressure on the formation energy of the vacancy, which is beyond the scope of this paper.

5. Conclusion

The interaction of H with a vacancy in Ni is investigated by means of DFT calculations. The strongest binding is found for an octahedral site in the vacancy O_1 (0.27 eV), with a negligible interaction in between O_1 sites. The site preference and binding energies are in excellent agreement with experiments and clarify the interpretation of the two peaks found by thermal desorption. Indeed, the second peak should be attributed to divacancies with an enhanced binding of 0.42 eV. At finite temperature, away from the infinite dilution, only O_1 is occupied due to a strong repulsion with T_1 sites. Mean field equations, validated by MC simulations, show that at $T = 300$ K, the trapping to the vacancy is strong. VH_5 and VH_6 are the dominant clusters beyond 100 ppm. These conditions correspond to typical H embrittlement experiments. Furthermore, even if the saturated vacancy is a seed for a local hydride, it is not stable, even at concentrations as high as 5000 ppm. The comparison between mean field equations and OLMC shows that thermal excitations have the tendency to destabilize the hydride. The absolute vacancy concentration is also estimated. At room temperature, the enrichment is of the order of 10 orders of magnitude with respect to thermal

vacancies, at 1000 ppm H. The consequences on vacancy-mediated diffusion need to be carefully examined as was previously done in Nb [37]. At high temperature (600 K), vacancies are noticeably decorated at much higher bulk concentrations (VH_1 concentration exceeds the equilibrium free vacancy concentration only beyond 500 ppm H). In comparison, the average H concentration in a PWR environment, in the presence of active stress corrosion cracks (i.e. frequent depassivation/repassivation events) is of the order of 40 ppm [11]. At first sight, it seems that H should not have noticeable effects in these conditions. Nevertheless, it is hard to determine experimentally the local H concentration, even using secondary ion mass spectrometry on samples oxidized in well-controlled conditions [15,16], let alone in the nanometer-scale process zone of a stress corrosion crack [13]. Local H concentrations beyond 1000 ppm cannot be excluded, making it necessary to consider the implication of SAVs in PWR conditions. At room temperature, on the contrary, trapping is very effective at H concentrations commonly used for embrittlement experiments. Nevertheless, the absolute SAV concentrations are still very low because of the large formation energy of the vacancy (E_v^f) in Ni. Furthermore, VH_6 clusters have repulsive effective interactions which guarantees that they do not cluster at low concentration. As a conclusion, it seems

highly unlikely that VH_n accumulate in the bulk to form crack nuclei, at least at high H concentrations. On the contrary, at any defect where E_v^f is small, the stability is enhanced. This suggests that out-of-equilibrium vacancies can diffuse over long distances and accumulate, for example, at GBs. We will give an example of this phenomenon in a forthcoming paper. We will also evaluate the influence of H on vacancy and metal diffusion at low temperature.

Acknowledgments

Appendix A. Details of the configurations included in the analytical model

Table A.4 gives all the information used to calculate the VH_n concentrations as a function of the bulk concentration and the temperature using the mean field formulas:

$$\frac{C_{bulk}}{1 - C_{bulk}} = e^{-\mu^*/k_B T}$$

$$C_{VH_k} = n_{VH_k} e^{-\left(E_f^{VH_k} + k\mu^*\right)/k_B T} \qquad (A.1)$$

Note that the number of configurations given is reduced to those of low formation energies. These energies are approximate values calculated from the average segregation energies and the pair interaction energies because they were shown to be weakly configuration dependent; therefore, the cluster formation energies are accurately reproduced but the configuration dependence is neglected. These energies are not the result of individual cluster calculations. This approximation enables comparison with the MC simulations on the rigid lattice, which, in return, confirms that the correct clusters have been selected for the model.

Furthermore, the VH_n concentrations given can be used to calculate the solute excess at vacancies and, from this, the free energy of formation of the defects, as a function of the H chemical potential. The decrease of this free energy with the H chemical potential follows that given in Fig.1 of Ref. [38]. The model we present is therefore fully coherent with the thermodynamic approach based on the defactant concept.

Table A.4
The number of H atoms involved in the cluster (k), the cluster configuration, the corresponding formation energy ($E_f^{VH_k}$ in eV) and the number of variants (n_{VH_k}) are presented.

k	Configuration	$E_f^{VH_k}$	n_{VH_k}
0		1.790	1
1	O_1	1.517	6
1	T_1	1.568	8
2	$2O_1$	1.244	15
2	$O_1 T_1$	1.295	24
2	$2T_1$	1.346	16
2	$O_1 T_1^*$	1.542	24
3	$3O_1$	0.971	20
3	$2O_1 T_1$	1.022	24
3	$O_1 2T_1$	1.073	12
3	$3T_1$	1.344	8
4	$4O_1$	0.698	15
4	$3O_1 T_1$	0.749	8
5	$4O_1 O_2$	0.598	120
6	$4O_1 2O_2$	0.498	420
7	$4O_1 3O_2$	0.398	840
5	$5O_1$	0.425	6
6	$5O_1 O_2$	0.325	48
7	$5O_1 2O_2$	0.225	168
8	$5O_1 3O_2$	0.125	336
6	$6O_1$	0.152	1
7	$6O_1 O_2$	0.052	8
8	$6O_1 2O_2$	−0.048	28
9	$6O_1 3O_2$	−0.148	56
10	$6O_1 4O_2$	−0.248	70
11	$6O_1 5O_2$	−0.348	56
12	$6O_1 6O_2$	−0.448	28
13	$6O_1 7O_2$	−0.548	8
14	$6O_1 8O_2$	−0.648	1

* Obtained with one T_1-O_1 first neighbor interaction.

References

[1] Fukai Y. The metal-hydrogen system: basic bulk properties. 2nd ed. Berlin: Springer-Verlag; 2003.
[2] Myers S, Baskes M, Birnbaum H, Corbett J, DeLeo G, Estreicher SK, et al. Rev Mod Phys 1992;64:559.

[3] Besenbacher F, Bøttiger J, Myers S. J Appl Phys 1982;53:3536.

[4] Tateyama Y, Ohno T. Phys Rev B 2003;67:174105.

[5] Wolverton C, Ozolins V, Asta M. Phys Rev B 2004;69:144109.

[6] Ismer L, Park MS, Janotti A, de Walle CV. Phys Rev B 2009;80:184110.

[7] Nazarov R, Hickel T, Neugebauer J. Phys Rev B 2010;82:224104.

[8] Nordlander P, Norskov J, Besenbacher F, Myers S. Phys Rev B 1989;40:1990.

[9] Fukai Y, Mizutani M, Yokota S, Kanazawa M, Miura Y, Watanabe T. J Alloys Compd 2003;356–357:270.

[10] Fukai Y, Shizuku Y, Kurokawa Y. J Alloys Compd 2001;329:195.

[11] Rios R, Magnin T, Noel D, de Bouvier O. Metall Mater Trans A 1995;26A:925.

[12] Takai K, Shoda H, Suzuki H, Nagumo M. Acta Mater 2008;56:5158.

[13] Sennour M, Laghoutaris P, Guerre C, Molins R. J Nucl Mater 2009;393:254.

[14] Dugdale H, Armstrong DEJ, Tarleton E, Roberts SG, Lozano-Perez S. Acta Mater 2013;61:4707.

[15] Jambon F, Marchetti L, Jomard F, Chêne J. J Nucl Mater 2011;414:386.

[16] Jambon F, Marchetti L, Jomard F, Chêne J. Solid State Ionics 2013;231:69.

[17] Hayashi E, Kurokawa Y, Fukai Y. Phys Rev Lett 1998;80:5588.

[18] Kresse T, Li Y, Boll T, Borchers C, Choi P, Al-Kassab T, et al. Scr Mater 2013;69:424.

[19] Kabir M, Lau T, Lin X, Yip S, Vliet KV. Phys Rev B 2010;82:134112.

[20] Fu C, Meslin E, Barbu A, Willaime F, Oison V. Solid State Phenom 2008;139:157.

[21] Kresse T, Borchers C, Kirchheim R. Scr Mater 2013;69:690.

[22] Kresse G, Hafner J. Phys Rev B 1993;47:558.

[23] Kresse G, Joubert D. Phys Rev B 1999;59:1758.

[24] Wang Y, Perdew JP. Phys Rev B 1991;44:13298.

[25] Monkhorst H, Pack J. Phys Rev B 1976;13:5188.

[26] Angelo J, Moody N, Baskes M. Model Simul Mater Sci Eng 1995;3:289.

[27] Tanguy D, Mareschal M. Phys Rev B 2005;72:174116.

[28] Connétable D, Wang Y, Tanguy D. J Aloys Compd 2014. accepted for publication.

[29] Fukai Y. J Alloys Compd 2003;356-357:263.

[30] Chêne J, Brass A. Met Trans A 2004;35A:457.

[31] van de Walle A, Ceder G. Rev Mod Phys 2002;74:11.

[32] Ozoliņš V, Asta M. Phys Rev Lett 2001;86:448.

[33] Song J, Curtin W. Acta Mater 2011;59:1557.

[34] Pezold JV, Lymperakis L, Neugebauer J. Acta Mater 2011;59:2969.

[35] Ullmaier H, editor. Atomic point defects in metals: crystal and solid state physics, vol. 25. Berlin: Springer-Verlag; 1991.

[36] Kraftmakher Y. Phys Rep 1998;299:79.

[37] Iida T, Yamazaki Y, Kobayashi T, Iijima Y, Fukai Y. Acta Mater 2005;53:3083.

[38] Kirchheim R. Acta Mater 2007;55:5139.